Section A-Research paper

ISSN 2063-5346

Influence of Shoulder-to-Probe Diameter Ratio on Mechanical and Microstructural Properties of Aluminum Sheets Joined by Bobbin Tool Friction Stir Welding

Hammad T. Elmetwally[1], Nabil K. Hassan[1], M. N. El-Sheikh[1], Ayman Ali Abd-Eltwab[2*] and Mahmoud E. Abdullah[1*]

[1]Mechanical Department, Faculty of Technology and Education, Beni-Suef University, Beni-Suef 62511, Egypt.

[2]*Mechanical Engineering Department, Faculty of Engineering, Beni-Suef University, Beni-Suef* 62511, *Egypt*

[*] Corresponding author Phone:002-01005728351, Mail: AymanAli@eng.bsu.edu.eg

E-mail: mmgzmhammad@gmail.com

E-mail: Nabil.kamal.iec83@gmail.com

E-mail: Elsheikh53@yahoo.com

E-mail: iec.mahmoud@gmail.com

Abstract

Solid-state welding of aluminum has become increasingly popular in recent years due to its ability to create strong joints without the need for fillers or external heat source. The use of a Bobbin tool can increase the efficiency and productivity of friction stir welding. The geometry of the tool plays a significant role in improving the mechanical and microstructural properties of the welded joint. To study the effect of Bobbin tool geometry, four different shoulder-to-probe diameter ratios were tested with a constant probe diameter of 5mm and pure aluminum sheets 3mm thick were used for the welded specimens. The welding conditions included a constant tool rotational speed of 653 rpm and a constant tool traverse speed of 44 mm/min. The thermal cycles, microstructure, and mechanical properties of the welded specimens were evaluated through various tests including microstructural analysis, fracture morphology examination via OM and SEM images, tensile tests, and microhardness tests. The experimental results showed that the fracture for the stronger specimen obtained when the shoulder to probe ratio was 2 and occurred far away from the welding nugget on the advancing side. On other hand, the fracture for the weakest specimen is produced when the shoulder to probe ratio was 3.5 and occurred in the stir zone center. The maximum joint strength and hardness were obtained at the minimum tool ratio due to dynamic recrystallization, fine particles, and homogenous structure present in both welding nugget and base metal. The weakest specimen showed voids, shallow and deep dimples, as well as many precipitates and cavities due to non-equilibrium material flow. Finally, it was observed that ductile fracture mode was present in optimum samples while brittle fracture mode was present in weakest samples.

Keywords: FSW, Bobbin Tool, Tool Ratio, Thermal Cycle, Microstructure, Ductile Fracture

1. Introduction

Friction stir welding (FSW) is a commonly used method for joining various metals and their alloys that are difficult to weld using traditional methods due to non-compositional homogeneity or differences in base metal properties [1]. The principle of FSW relies on the heat generated as a result

ISSN 2063-5346

of the contact between the welding tool and the workpiece surface, with the welding temperature being below the melting point of the base material [2]. In recent years, FSW has become a popular choice for welding aluminum sheets and plates, as well as their alloys, due to its ability to prevent the formation of oxidation layers. Additionally, FSW is classified as a low-cost welding technique [3].

The FSW tool typically consists of a shoulder and a probe. The tool shoulder serves as the primary component for retaining the frictional heat generated on the top surface, while the tool probe is utilized to enhance the interface between parent metals in the stir zone [4], [5]. However, it's important to note that the length of the probe is limited to 0.9 times the thickness of the base metal to prevent it from penetrating or creating a groove in the backing plate [6]. Bobbin Tool Friction Stir Welding (BT-FSW) is an advancement of conventional friction stir welding (CFSW). BT-FSW is a self-reacting welding tool that offers several advantages over CFSW, including zero downward force, improved joint quality, increased productivity, and prevention of welding root defects [7], [8–11]. The manufacturing process for bobbin tools involves using a dual shoulder and a single probe. The probe is fixed axially between dual shoulders to adjust their distance. Precision and meticulous attention to detail are required during manufacturing to ensure each tool's superior quality and reliable performance over time [12].

Previous studies have explored various enhancements and welding parameters for BT-FSW. For example, Yang et al. [13] compared the welding strength of welded specimens by CFSW and BT-FSW for 6061-T4 and found that the BT-FSW process produced defect-free joints. Esmaily et al. [14] studied the behavior of AA6005-T6 welded specimens by both CFSW and BT-FSW and found that the latter can produce a higher peak temperature due to its larger surface area and ability to apply more force to the workpiece, contributing to higher peak temperatures. However, it's important to note that peak temperature alone doesn't necessarily determine the overall effectiveness or quality of a welding process. Xu et al. [8] investigated the mechanical properties and fracture behavior of welded specimens using two different techniques: CFSW and BT-FSW. They reported that the temperature gradient along the thickness direction of CFSW joints was nonuniform, while the temperature of the lower shoulder-affected zones was slightly higher than that of the upper shoulder-affected ones for the BT-FSW joints. The microhardness distribution was like a W-shape that indicated lower hardness in the Heat Affected Zone (HAZ). Li et al. [15] investigated the impact of rotational speed on welding aluminum alloy 6082-T6 using BT-FSW and found that an increase in rotational speed led to a corresponding rise in welding temperature. Fuse and Badheka [16] conducted a research study to examine the impact of shoulder-to-probe diameter ratio (2:1, 2.75:1, 3:1) of BT-FSW on welding strength and microstructure properties of AA 6061-T6 aluminum. The findings revealed that a defect-free joint can be achieved by utilizing a shoulder-to-probe ratio of 3:1, which requires maintaining an appropriate temperature estimated at 52.3% of the melting temperature of aluminum. Bokov et al. [17] conducted research on the impact of total contact area on heat generation during the welding of dissimilar materials. They reported that the total contact tool profile is a significant parameter that affects welding temperature, given the difference in thermal diffusivity of the parent material. Chupradit et al [18] investigated the effect of tool contact area on heat generation and mechanical working of the welding nugget. Their study revealed a strong linear correlation between contact area and welding temperature, with a confidence level of 99%. Fuse and Badheka [6] used H13 steel to manufacture the bobbin tool with a shoulder-to-probe ratio of 3 to weld AA 6061-T6. They found that mechanical properties at the heat-affected zone were lower

ISSN 2063-5346

compared to the strength of the base metal. Wang et al. [9] conducted a study to examine how rotational speed affects strength and microstructure in welded nuggets using BT-FSW. The findings indicated that there was a direct relationship between rotational speed and welding efficiency, with an 80% welding efficiency achieved at a rotational speed of up to 800 rpm. However, as rotational speed increased to 1000 rpm, welding efficiency decreased. Li et al. [19] studied tool design improvements for achieving defect-free welding nuggets. They used high traveling speeds ranging from 200 mm/min to 600 mm/min along with a rotational speed of 600 rpm. It was found that high rotational speeds may cause damage to the welding tool while low traveling speeds caused tunnel defects in the stir zone. They support that contact area in FSW is one of the most crucial parameters for generating frictional heat.

Previous studies on the BT-FSW have focused on the effect of rotational and traverse speeds, probe shape, and a comparison between FSW and BT-FSW on the mechanical and microstructural properties of welded joints. However, limited consideration has been given to the effect of shoulder-to-probe ratio. Therefore, this experimental study aims to investigate the impact of shoulder-to-probe ratio on the thermal cycle, microstructural, and mechanical properties of aluminum joints.

2. Experimental procedures

The base metal used in this study is commercial aluminum with a thickness of 3 mm. Table (1) provides information on its chemical composition while table (2) presents its mechanical properties. All produced joints have dimensions of 200 *200 mm. The welding direction is parallel to the rolling direction of the original sheet metal, and experiments are conducted using a universal milling machine called “Milko-35r”. The welding tools are made from W302 steel bars with fixed probe diameter of 5 mm for all tools. However, shoulder diameters are varied to achieve different shoulder-probe diameter ratios (R) of 2, 2.5, 3, and 3.5 as shown in figure (1).

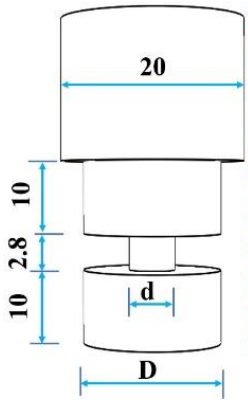

Tool	I	II	III	IV
D(mm)	10	12.5	15	17.5
d(mm)	5	5	5	5
Ratio	2	2.5	3	3.5

Fig. 1 Bobbin tool design.

The tool was machined to the selected dimensions and then hardened up to 52 HRC in order to increase its lifespan and prevent aluminum adhesion in the tool groove. Figure (2) displays the test rig description, welding procedure, tools manufacturing, and workpiece design. During the welding process, a thermos-detector-infrared camera (Bosh^{TM} GIS 1000 ^{o}C Professional) was used to

ISSN 2063-5346

measure the temperature and evaluate the thermal cycle of the welding process, as well as evaluate its impact on the mechanical properties of joints. The infrared beam was directed to the middle of the welding pass at the advancing side for temperature measurements along the welding pass. Tensile samples were designed according to ASTM-E8M standard with 2 mm/min cross head speed after completion of the welding process. All tensile tests were conducted using a universal testing machine QUASAR 100-VAV201 with a capacity of 100 KN. Microhardness was measured by a Vickers testing machine, VMH tester model number 1600-4981, with a standby time of 15 s and 500 gf. The fracture behaviors of tensile fractured surfaces were evaluated via scanning electron microscope (SEM), JSM-IT200. Macro and microstructural analysis were used to conduct tensile test results for both optimum case and lower-case specimen.

Table (1) Chemical composition (wt. %) of aluminum (as received)

Element	Fe %	Ti%	Sn%	Zn%	Pb%	Ga%	V%	Co%	Bi%	B%	AL
Wt.%	0.338	0.048	0.038	0.031	0.028	0.016	0.015	0.013	0.012	0.01	Bal.

Table (2) Tested Mechanical properties of as received aluminum.

Average Proof Stress (MPa)	Average UTS (MPa)	Average E %	Average Hardness (HV)
86	116	11	50±0.8

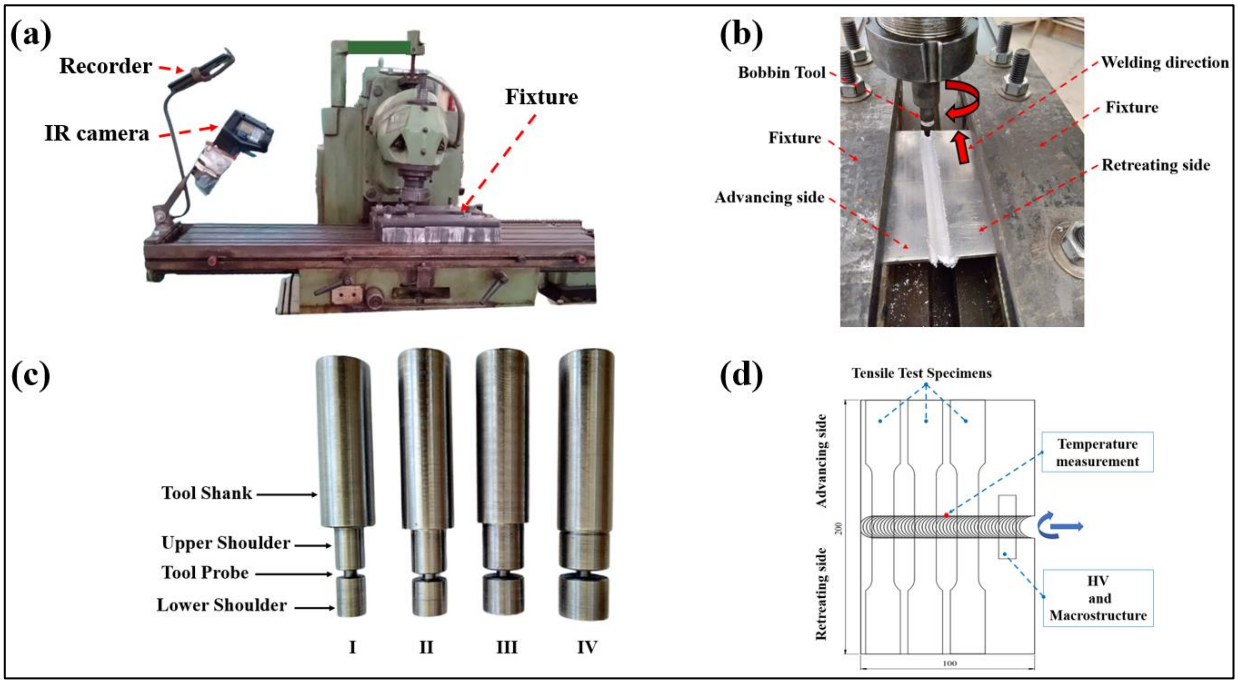

Fig. 2 a) Test Rig Description, b) welding process, c) Tools manufacturing, and, d) workpiece design

ISSN 2063-5346

3. Results and discussion

3.1 Thermal cycles

The transient temperature differences of the BFSW were evaluated through thermal cycles. Fig. 3 shows the effect of shoulder diameter to probe diameter on the thermal cycle. The thermal cycle is consistent with previously reported works [4], [18] and includes a heating region starting as the tool bites into the workpiece until the temperature rises to its peak value, followed by a cooling region until the end of the welding line. Table 3 presents peak temperature, heating and cooling rates for each tool ratio. Welding tools I, II, III, and IV recorded peak temperatures of 307℃, 310℃, 328℃, and 294℃ respectively. The heating rate was highest when using tool III (R=3) but lowest when using tool IV (R=3.5), with a difference of 12.7%. The same trend was observed for cooling rates, with a maximum difference of 13.9%, in agreement with other work [22]. As tool ratio increases, so does the contacted area between tool and workpiece, leading to increased friction-generated heating. However, when tool ratio exceeds 3, dissipated power in workpiece material increases and welding temperature at center of welding line decreases due to insufficient stirring caused by increase in stirred material volume (see Table 3).

Table 3: Peak temperature, heating rate, and cooling rate for different tool ratios.

Tool ratio (shoulder diameter/probe diameter)	R= 2.0 (Tool I)	R= 2.5 (Tool II)	R= 3.0 (Tool III)	R= 3.5 (Tool IV)
Peak Temperature (°C)	307	310	328	298
Heating Rate ($°CS^{-1}$)	4.21	4.32	4.52	4.01
Cooling Rate ($°CS^{-1}$)	1.67	1.68	1.80	1.58
Stirred material volume (mm^3)	176.72	309.25	471.24	662.68

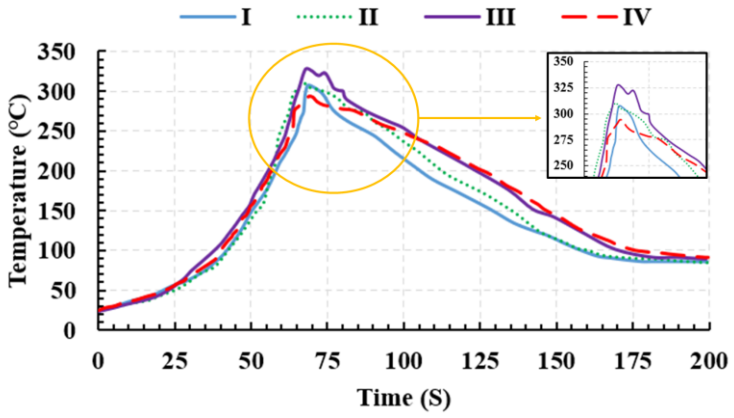

Fig. 3 Thermal cycles of BT-FSW process at different tool ratios

3.2 Surface morphology appearance, macrostructure, and microstructure

Fig. 4 shows the visual inspection of the welded specimen on the top surfaces for different tools. The optimum surface appearance is produced when the minimum tool ratio (R = 2) is used. The

ISSN 2063-5346

observation focused on the absence of flash defects around the welding line, indicating the discipline of the stirring process along the welding line. Low ripples are observed along the weld line except during tool inlet. When the tool ratio is increased to more than 2.5 (tools III & IV), many ripples are noticed around the welding line, and low surface roughness is obtained due to a large amount of material being deformed and stirred. Similar observations were obtained by other works [21-22] when studying traveling speeds' effect.

Fig. 5 and Fig. 6 show macrostructure and microstructure images of minimum and maximum tool ratios, respectively. Cross-sectional macrostructure images were taken with a stereomicroscope, while microstructure images were taken using a traditional optical microscope (OM). The main four welding regions, i.e., base metal (BM), heat affected zone (HAZ), thermo-mechanically affected zone (TMAZ), and stir zone (SZ), for both specimens can be easily recognized. As seen in Fig. 5a, a sharp transition between BM and nugget occurs on both sides (i.e., advanced side (AS) and retreating side (RS)), while maximum width of nugget zone is obtained in upper and bottom surfaces of specimen as it stirred with tool shoulder, and minimum width of nugget zone lies at middle slightly larger than pin diameter. Nugget shape is compatible with friction produced at contact areas between tool and workpiece. When sample was welded using tool IV (with maximum tool ratio R=3.5), a more diffuse transient region is present on both sides of specimen (Fig. 6a). Fig. 6a displays the ripple spaces that have increased at the top and bottom surfaces, along with the flash configuration on the advanced side. The dissimilar nugget shapes of the two specimens are attributed to different flow behaviors, degree of plastic deformation, contact, and friction heat produced from both upper and lower shoulders. The SZ is more refined than the base metal in both AS and RS. In the optimum welding specimen, both TMAZ and HAZ have a small narrow width due to welding variables' compatibility. The TMAZ welded by R=3.5 is considered abnormal due to low metal flow rate from AS to RS. Fig. 5(b-d) shows microstructure images of cross-sections of welded joints at different positions of optimum specimens, while Fig. 6(b-d) represents microstructure images of weakest specimens at TMAZ of RS, SZ, and TMAZ of AS. The heat-affected zone of the optimum specimen exhibits dynamic recrystallization structure under increasing temperature and stirring action (see Fig. 5c). The stir zone of the optimum specimen resembles sea waves taking rotational direction as shown in Fig. 5c. The thermos-mechanically affected zone (Fig. 5d) displays fine particle structure.

The microstructure of the specimen welded by tool IV showed a completely different structure in which material wrinkling was observed at TMAZ of the advancing side and the retreating side (Fig. 6b and Fig. 6d). Wrinkled material pattern indicates to poor or incomplete stirring action due to increase of the material static volume between the two shoulder when tool IV used. The stir zone exhibited fine, equiaxed microstructure (Fig. 5c and Fig. 6c). This is due to severe plastic deformation takes place at the pin area during welding [16].

ISSN 2063-5346

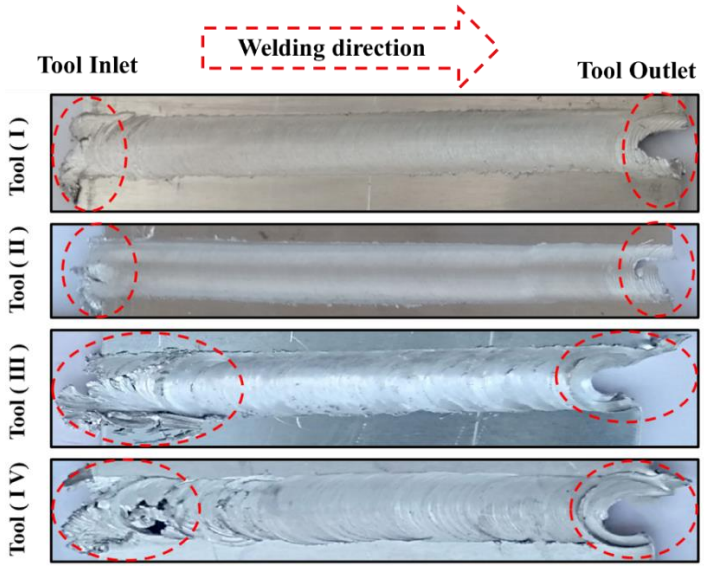

Fig. 4 Top view of the weld appearance with different tool ratios

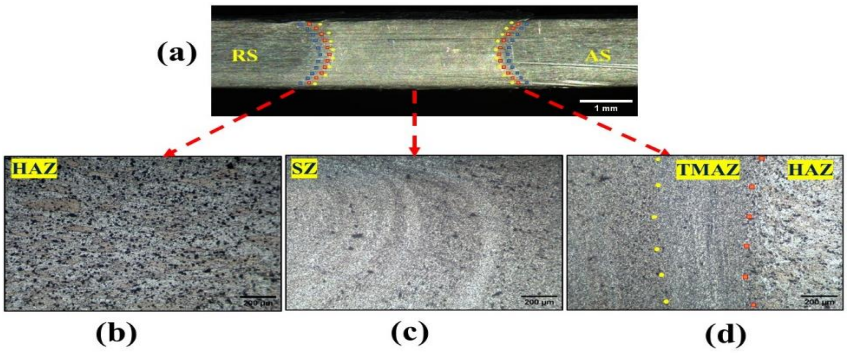

Fig. 5 Macro and Microstructure of the cross-section of the optimum welded joint (tool I); (a) macrostructure-stereo image, (b), (c) and (d) OM images of microstructure at different welding zones

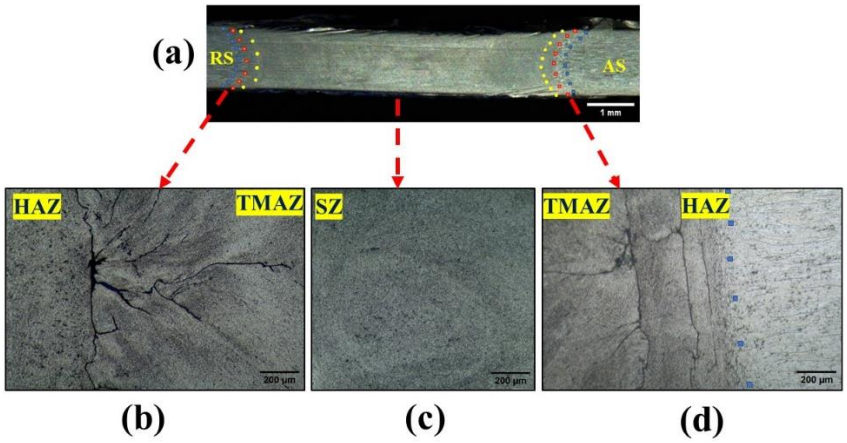

Fig. 6 Macro and Microstructure of the cross-section of the poor welded joint (tool IV); (a) macrostructure-stereo image, (b), (c) and (d) OM images of microstructure at different welding zones

ISSN 2063-5346

3.2 Mechanical properties

Fig. 7 displays the tensile results of joints created using different tool ratios, as well as those of the base metal (BM). It is evident that the overall mechanical properties decrease significantly with an increase in tool ratio. The highest proof stress and ultimate tensile stress values were obtained when the minimum tool ratio (R=2) was used. The maximum proof stress is 73.3% of the BM, while the maximum ultimate tensile stress is 89.7% of the BM. The maximum elongation was also achieved when using the minimum tool ratio (tool I), whereas the lowest average elongation in welded specimens was found when using a tool ratio of 3.5. These results can be explained by considering the recorded temperatures along the welding line and cooling rates. As temperature increases, cooling rate increases, leading to finer and harder grains in the stir zone, resulting in increased proof stress, ultimate tensile stress, and elongation percentage. Conversely, when temperatures are at their minimum values, cooling rate slows down, causing enlargement and coarsening of metal grains at stir zone boundaries, particularly on the advancing side, leading to reduced hardness and weakened joints with decreased elongation. The difference in grain hardness at stir zone boundaries creates an irregular composition that weakens joints and reduces their tensile resistance.

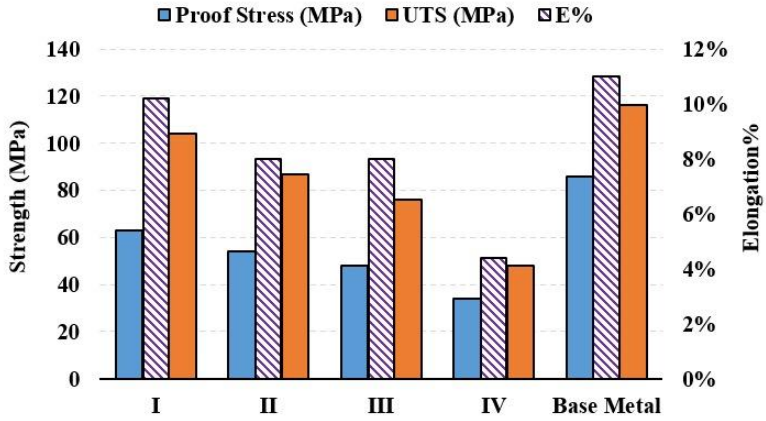

Fig. 7 Mechanical properties of the welded joints for different tool ratios

The microhardness readings along the welding line, including SZ, TMAZ, and HAZ, are displayed in Fig. 7. The microhardness results indicate that the minimum hardness values are obtained at a distance of 2mm around the zero line and reach their maximum at 6mm on the advancing side and 5mm on the retreating side. The difference between the maximum and minimum hardness values is 8, 6, 7, and 12 HV for tools I, II, III, and IV respectively. This suggests that there is a more inhomogeneous composition in the SZ of tool IV than in tools I, II, and III. These results are consistent with the tensile test results and previous microstructure analysis. The average microhardness of welded specimens using tools I, II, and III was found to be 51±4.3, 51±4.28, and 51±4.58 respectively. In contrast, specimens welded using tool IV had an average hardness of 44±3.53. With the exception of specimen IV, all tool ratios showed higher average hardness values than those of the base metal which agrees with peak temperature results. The average microhardness results suggest that the average strength of the stir zone may be similar for tools I-III while samples welded using tool IV have lower strength on average compared to other tools.

ISSN 2063-5346

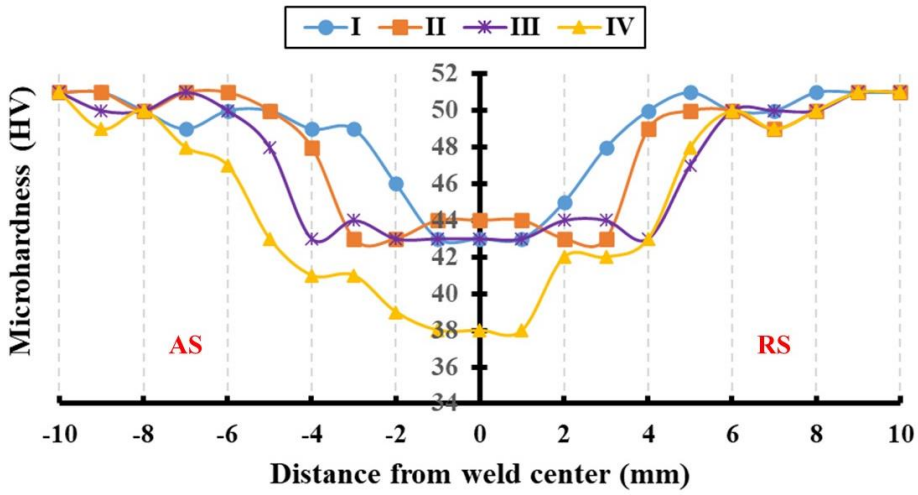

Fig. 7 Vickers Microhardness of welded specimens along the welding line

3.4 Fracture morphology

Fig. 8 displays the fracture location of welded specimens following tensile tests at varying tool ratios. When the specimen was welded using a tool ratio of R=2, the fracture occurred solely at the base metal. However, when the tool ratio was increased to 2.5, the fracture was produced at the interface between the base metal and welding nugget zone of the advanced side. By further increasing the tool ratio to 3, the fracture occurred at the interface between the base metal and welding nugget zone of the retreating side. In cases where R=3.5, the fracture occurred in the weld stir zone near the advancing side, indicating low penetration of weld into base metal. The positions of fractures shown in Fig. 8 suggest that strongest and defect-free joints were produced at lowest tool ratio while weakest joint (fracture inside stir zone) resulted at highest tool ratio.

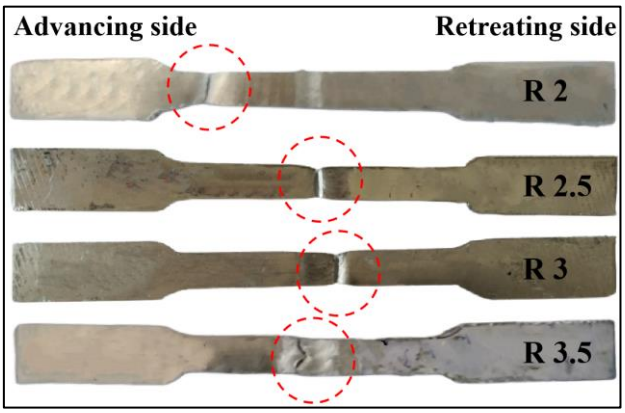

Fig. 8 Fracture location of welded specimens for different tool ratios.

The SEM was used to evaluate the welding nugget of the optimum welded specimen on both the thickness and surface, as depicted in Fig. 9. The results showed that the refined grains were a result of appropriate dynamic recrystallization in the stir zone. Additionally, on the surface of the stir zone, there was a regular coordination of ripples with some flying edges. The ripple spacing ranged from 8 to 10.11 µm, with an average of 9.27 ± 1.16 µm.

ISSN 2063-5346

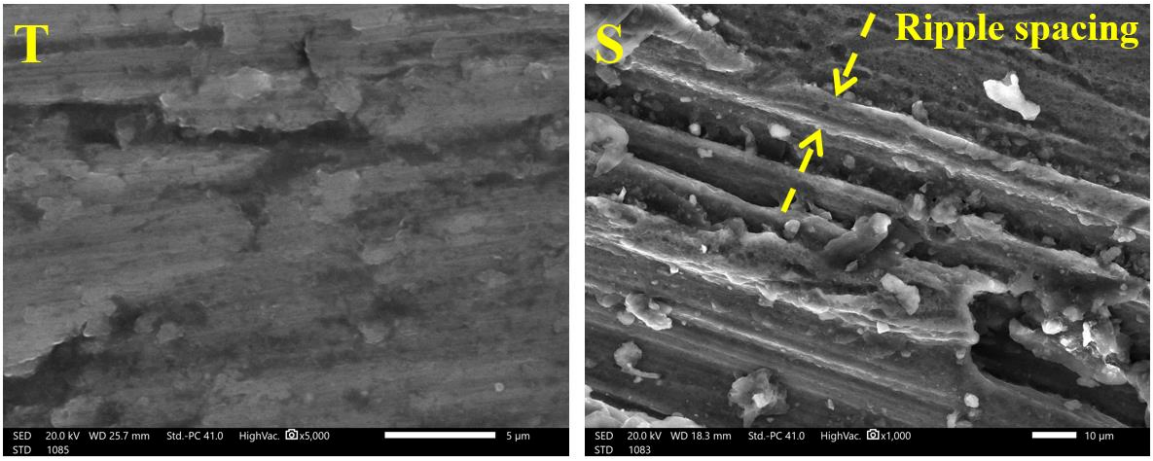

Fig. 9 SEM images of stir zone of the specimen welded by Tool (I). T: cross section, S: surface.

Fig. 10 displays the fractured surface of the specimens in the stir zone at the advancing side. The fracture surface that exhibited higher elongation was mainly dominated by fine dimples with few voids, signifying a ductile mechanism as observed in Fig. 10 for samples I and II. Both samples showed cleavage and ductile modes of failure. However, in the case of sample III and sample IV, voids and cavities were found in more positions, along with deep and shallow dimples where many precipitates were observed at the bottom of these dimples. The presence of these defects in both samples III and IV indicates a brittle fracture mode which can be attributed to slow cooling rates [10]. Although the fracture of samples III and IV appeared to be ductile, earlier failure was produced in the welding zone due to the absence of equilibrium between the mechanical working of the welding tool and heat generation. Therefore, cavities are enough to cause a failure in the welding zone due to non-optimal material flow conditions [9].

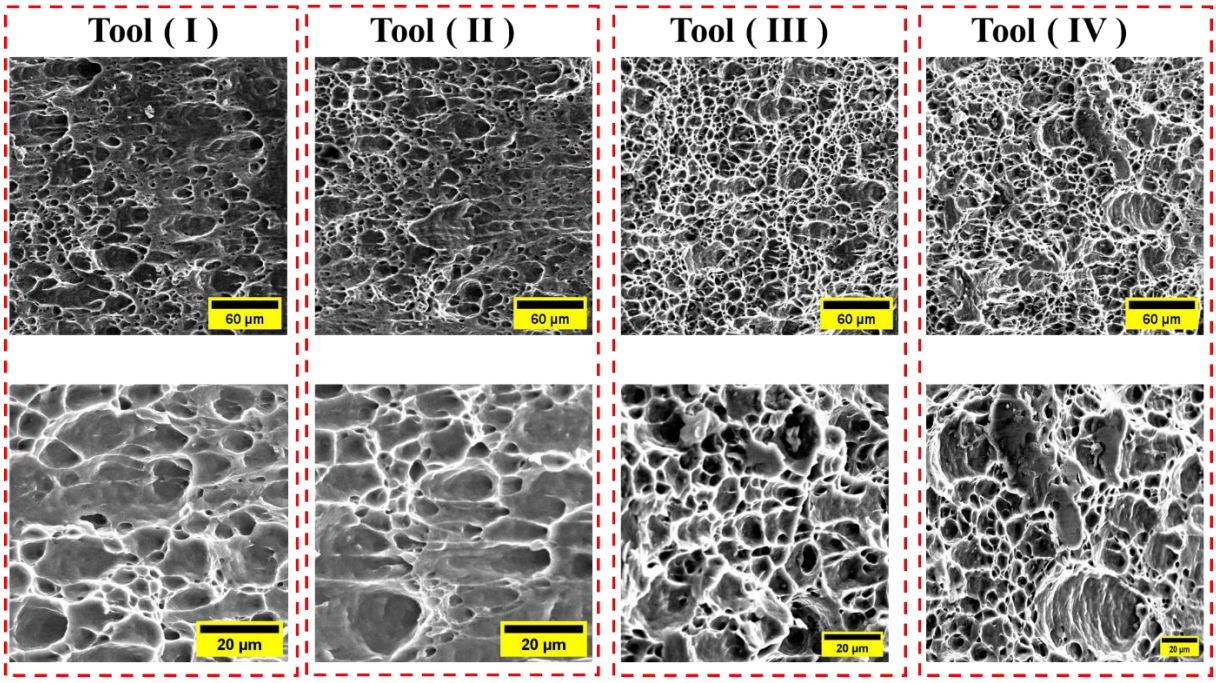

Fig. 10 SEM image of Fracture surface of specimen by different tool ratio.

4. Conclusions

The specimens were successfully welded using bobbin tools friction stir welding at different tool ratios. It was discovered that the tool ratio is a crucial factor in controlling welding efficiency. The study yielded the following conclusions:

- Heating cycles at different tool ratios showed that peak temperature, heating rates, and cooling rates reached their maximum values when a tool ratio of 3 was used, while they were minimum when a tool ratio of 3.5 was used. At the largest tool ratio, a higher material volume was stirred, and a higher amount of heat was dissipated.
- The optimum appearance of the joint was observed when the minimum tool ratio was used, indicating a defect-free surface. However, many ripples and surface cracks were observed at the maximum tool ratio (R=3.5). Microstructural analysis revealed dynamic recrystallization and fine particles in the SZ for the R=2 case; however, material wrinkling was observed at TMAZ for the maximum tool ratio case (R=3.5) due to poor or incomplete stirring.
- Superior mechanical properties were obtained at the minimum tool ratio due to dynamic recrystallization, fine particles, and homogenous structure of the welding nugget and base metal. Microhardness results were compatible with peak temperature and cooling rates.
- The strongest specimen (R=2) fractured at the advanced side of the base metal while it produced at the welding nugget in the case of the weakest specimen (R=3.5). Fracture morphology showed voids, shallow and deep dimples, and many precipitates and cavities due to non-equilibrium of material flow when using maximum tool ratio. The fracture mode of the optimum specimen referred to ductile fracture while that of weakest specimen looked like brittle fracture due to non-optimal material flow conditions.

Author Contributions:

The contribution of the authors is as follows; Mohamed N. Elsheikh designs the main idea. Nabil K. Hassan prepared the test-rig component. Mahmoud E. Abdullah, Nabil K. Hassan, Mohamed N. Elsheikh, and Hammad T. Elmetwally made experimental works. Nabil K. Hassan and Mahmoud E. Abdullah wrote a draft copy. Hammad T. Elmetwally and Mahmoud E. Abdullah collected the data and analyzed it. Mohamed N. Elsheikh review and revised the manuscript.

Funding: This research received no external funding.

Conflicts of Interest: The authors declare no conflict of interest.

Acknowledgment: The authors extend their thanks and appreciation to the technical staff, Faculty of Technology and Education, Beni-Suef University.

Availability of data and materials and Consent for publication: Not applicable.

References

1. Bocchi, S.; D'Urso, G.; Giardini, C. The Effect of Heat Generated on Mechanical Properties of Friction Stir Welded Aluminum Alloys. *Int. J. Adv. Manuf. Technol.* **2021**, *112*, 1513–1528, doi:10.1007/s00170-020-06462-9.

2. Senapati, N.P.; Bhoi, R.K. Improving the Strength of Friction-Stir-Welded Joints of AA1100 Alloy. *J. Mater. Eng. Perform.* **2021**, *30*, 510–521, doi:10.1007/s11665-020-05331-6.

3. Srivastava, M.; Rathee, S.; Maheshwari, S.; Noor Siddiquee, A.; Kundra, T.K. A Review on Recent Progress in Solid State Friction Based Metal Additive Manufacturing: Friction Stir Additive Techniques. *Crit. Rev. Solid State Mater. Sci.* **2019**, *44*, 345–377, doi:10.1080/10408436.2018.1490250.

4. Khalaf, H.I.; Al-Sabur, R.; Abdullah, M.E.; Kubit, A.; Derazkola, H.A. Effects of Underwater Friction Stir Welding Heat Generation on Residual Stress of AA6068-T6 Aluminum Alloy. *Materials (Basel).* **2022**, *15*, 2223, doi:10.3390/ma15062223.

5. Fuse, K.; Badheka, V. Bobbin Tool Friction Stir Welding: A Review. *Sci. Technol. Weld. Join.* **2019**, *24*, 277–304, doi:10.1080/13621718.2018.1553655.

6. Fuse, K.; Badheka, V. Hybrid Self-Reacting Friction Stir Welding of AA 6061-T6 Aluminium Alloy with Cooling Assisted Approach. *Metals (Basel).* **2020**, *11*, 16, doi:10.3390/met11010016.

7. Wang, G.Q.; Zhao, Y.H.; Tang, Y.Y. Research Progress of Bobbin Tool Friction Stir Welding of Aluminum Alloys: A Review. *Acta Metall. Sin. (English Lett.* **2020**, *33*, 13–29, doi:10.1007/s40195-019-00946-8.

8. Xu, W.; Luo, Y.; Zhang, W.; Fu, M. Comparative Study on Local and Global Mechanical Properties of Bobbin Tool and Conventional Friction Stir Welded 7085-T7452 Aluminum Thick Plate. *J. Mater. Sci. Technol.* **2018**, *34*, 173–184, doi:10.1016/j.jmst.2017.05.015.

9. Wang, F.F.; Li, W.Y.; Shen, J.; Hu, S.Y.; dos Santos, J.F. Effect of Tool Rotational Speed on the Microstructure and Mechanical Properties of Bobbin Tool Friction Stir Welding of Al-Li Alloy. *Mater. Des.* **2015**, *86*, 933–940, doi:10.1016/j.matdes.2015.07.096.

10. Yang, C.; Ni, D.R.; Xue, P.; Xiao, B.L.; Wang, W.; Wang, K.S.; Ma, Z.Y. A Comparative Research on Bobbin Tool and Conventional Friction Stir Welding of Al-Mg-Si Alloy Plates. *Mater. Charact.* **2018**, *145*, 20–28, doi:10.1016/j.matchar.2018.08.027.

11. Esmaily, M.; Mortazavi, N.; Osikowicz, W.; Hindsefelt, H.; Svensson, J.E.; Halvarsson, M.; Martin, J.; Johansson, L.G. Bobbin and Conventional Friction Stir Welding of Thick Extruded AA6005-T6 Profiles. *Mater. Des.* **2016**, *108*, 114–125, doi:10.1016/j.matdes.2016.06.089.

12. Fuse, K.; Badheka, V. Bobbin Tool Friction Stir Welding: A Review. *Sci. Technol. Weld. Join.* **2019**, *24*, 277–304, doi:10.1080/13621718.2018.1553655.

13. Yang, C.; Ni, D.R.; Xue, P.; Xiao, B.L.; Wang, W.; Wang, K.S.; Ma, Z.Y. A Comparative Research on Bobbin Tool and Conventional Friction Stir Welding of Al-Mg-Si Alloy Plates. *Mater. Charact.* **2018**, *145*, 20–28, doi:10.1016/j.matchar.2018.08.027.

14. Esmaily, M.; Mortazavi, N.; Osikowicz, W.; Hindsefelt, H.; Svensson, J.E.; Halvarsson, M.; Martin, J.; Johansson, L.G. Bobbin and Conventional Friction Stir Welding of Thick Extruded AA6005-T6 Profiles. *Mater. Des.* **2016**, *108*, 114–125, doi:10.1016/j.matdes.2016.06.089.

15. Li, Y.; Sun, D.; Gong, W. Effect of Tool Rotational Speed on the Microstructure and Mechanical Properties of Bobbin Tool Friction Stir Welded 6082-T6 Aluminum Alloy. *Metals (Basel).* **2019**, *9*, doi:10.3390/met9080894.

ISSN 2063-5346

16. Fuse, K.; Badheka, V. Effect of Shoulder Diameter on Bobbin Tool Friction Stir Welding of AA 6061-T6 Alloy. *Mater. Today Proc.* **2020**, *42*, 810–815, doi:10.1016/j.matpr.2020.11.366.

17. Bokov, D.O.; Jawad, M.A.; Suksatan, W.; Abdullah, M.E.; Świerczyńska, A.; Fydrych, D.; Derazkola, H.A. Effect of Pin Shape on Thermal History of Aluminum-Steel Friction Stir Welded Joint: Computational Fluid Dynamic Modeling and Validation. *Materials (Basel).* **2021**, *14*, 7883, doi:10.3390/ma14247883.

18. Chupradit, S.; Bokov, D.O.; Suksatan, W.; Landowski, M.; Fydrych, D.; Abdullah, M.E.; Derazkola, H.A. Pin Angle Thermal Effects on Friction Stir Welding of AA5058 Aluminum Alloy: CFD Simulation and Experimental Validation. *Materials (Basel).* **2021**, *14*, 7565, doi:10.3390/ma14247565.

19. Li, G.H.; Zhou, L.; Luo, S.F.; Dong, F.B.; Guo, N. Quality Improvement of Bobbin Tool Friction Stir Welds in Mg-Zn-Zr Alloy by Adjusting Tool Geometry. *J. Mater. Process. Technol.* **2020**, *282*, doi:10.1016/j.jmatprotec.2020.116685.

20. Esmaeili, A.; Givi, M.K.B.; Rajani, H.R.Z. A Metallurgical and Mechanical Study on Dissimilar Friction Stir Welding of Aluminum 1050 to Brass (CuZn30). *Mater. Sci. Eng. A* **2011**, *528*, 7093–7102, doi:10.1016/j.msea.2011.06.004.

21. Zhao, Y.; Wang, C.; Dong, C. Microstructural Characteristics and Mechanical Properties of Water Cooling Bobbin-Tool Friction Stir Welded 6063-T6 Aluminum Alloy. *MATEC Web Conf.* **2018**, *206*, doi:10.1051/matecconf/201820603002.

22. Khan, N.Z.; Khan, Z.A.; Siddiquee, A.N. Effect of Shoulder Diameter to Pin Diameter (D/d) Ratio on Tensile Strength of Friction Stir Welded 6063 Aluminium Alloy. *Mater. Today Proc.* **2015**, *2*, 1450–1457, doi:10.1016/j.matpr.2015.07.068.